

# Repulsive Bose-Einstein condensate in Periodic Potentials: Wells, Barriers, and Standing Waves

J. C. Bronski<sup>1</sup>, L. D. Carr<sup>2</sup>, R. Carretero-González<sup>3</sup>, B. Deconinck<sup>4</sup>, J. N. Kutz<sup>4\*</sup>, and K. Promislow<sup>3</sup>

<sup>1</sup>*Department of Mathematics, University of Illinois Urbana-Champaign, Urbana, IL 61801, USA*

<sup>2</sup>*Department of Physics, University of Washington, Seattle, WA 98195-1560, USA*

<sup>3</sup>*Department of Mathematics, Simon Fraser University, Burnaby, B.C., CANADA V5A 1S6*

<sup>4</sup>*Department of Applied Mathematics, University of Washington, Seattle, WA 98195-2420, USA*

Goal – new solutions, stability, applications: Audience – physics community: theorists and experimentalists: Time – by Oct. 1.

## I. INTRODUCTION

Recent experiments on dilute-gas Bose-Einstein condensate (BEC) have generated great interest in both the theoretical and experimental physics community. This interest is motivated by the ability to study quantum phenomena from a macroscopic viewpoint. The BEC has been generated by many groups using different gases which are cooled to very low temperatures and confined in magnetic fields or standing light waves. In this limit, a mean-field description for the macroscopic wavefunction can be constructed from the Hartree-Fock approximation [1]. For quasi-one-dimensional configurations, the mean-field of the BEC is modeled by the cubic nonlinear Schrödinger equation (NLS) with a potential [3–5]. Although the NLS is well studied, the various traps which are used to confine the BEC have led to new solutions of the NLS which include the potential explicitly [2,6]. The content of this paper applies to standing wave confinement of the BEC. BECs trapped in such a way have been used to study phase coherence [9] and matter-wave diffraction [10] and have been predicted to have applications in quantum logic [11], matter-wave transport [12], and for matter-wave gratings. We present new solutions pertaining to the BEC with a standing wave potential. Their dynamics, stability, and confinement under perturbations is studied both analytically and numerically.

Exact solutions of the NLS with a periodic potential were obtained for the Kronig-Penney potential [13] and some researchers have used a Bloch function description [14]. We construct new solutions with a more general periodic potential corresponding to a quasi-one-dimensional repulsive BEC trapped in an external potential. The governing equation is given by the nonlinear Schrödinger equation [3]

$$i\psi_t = -\frac{1}{2}\psi_{xx} + |\psi|^2\psi + V(x)\psi, \quad (1)$$

where  $\psi(x, t)$  represents the macroscopic wave function of the condensate and  $V(x)$  is an experimentally generated macroscopic potential. The two primary potentials constructed to date include: the harmonic well which is

generated experimentally from magneto-optical traps [8], and a periodic potential which is created from standing light waves [9]. A large class of periodic potentials is given by

$$V(x) = -V_0 \operatorname{sn}^2(x, k) \quad (2)$$

where  $\operatorname{sn}(x, k)$  denotes the Jacobian elliptic sine function [15] with elliptic modulus  $0 \leq k \leq 1$ . Since  $\operatorname{sn}(x, k)$  is periodic in  $x$  with period  $4K(k) = 4 \int_0^{\pi/2} d\alpha / \sqrt{1 - k^2 \sin^2 \alpha}$ ,  $V(x)$  is periodic in  $x$  with period  $2K(k)$ . In the limit  $k \rightarrow 1^-$ ,  $V(x)$  becomes an array of well-separated hyperbolic secant potential barriers or wells, while in the limit  $k \rightarrow 0^+$  it becomes purely sinusoidal. We note that for most intermediate values (e.g.  $k = 1/2$ ) the potential closely resembles sinusoidal behavior and thus provides a good approximation to the standing wave potential generated experimentally [9]. The potential is plotted in Fig. 1 for values of  $k = 0, 0.9, 0.999$  and  $0.999999$ . Only for  $k$  very near unity (e.g.  $> 0.999$ ) does the solution start to appear visibly elliptic. The freedom in choosing  $k$  allows great flexibility in considering a wide variety of physically realizable periodic potentials.

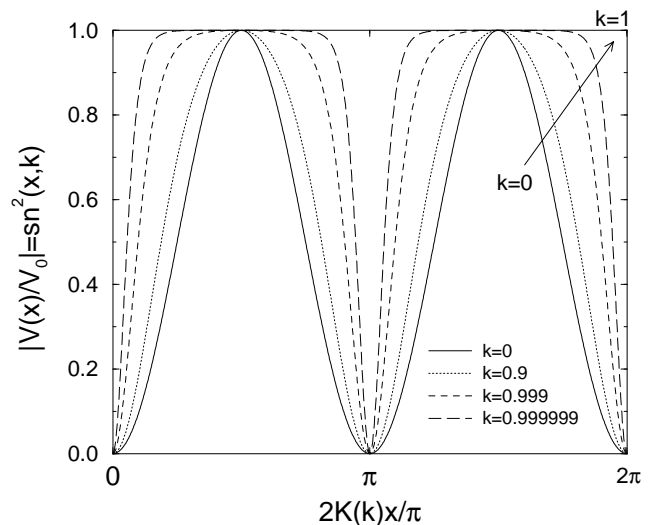


FIG. 1. The change in  $\text{sn}^2(x, k)$  for varying values of  $k$ . Note that the  $x$ -coordinate has been scaled by the period of the elliptic function. This period approaches infinity as  $k \rightarrow 1$ .

The outline of this paper is as follows: in the next section we derive and consider various properties and limits of two types of explicit solutions of Eq. (1) with (2). Section III develops the analytic framework for the linear stability properties of the new solutions of Sec. II. The stability results are confirmed by numerical computations. In certain cases, the stability analysis is intractable and we rely solely on simulations to determine stability. Nonstationary solutions are considered numerically in Sec. IV. This includes breathers and time- and space-periodic solutions. The possible applications of these new solutions and their relationship to experiment are considered in Sec. V with emphasis given to the possible construction of such solutions from existing experimental techniques. We conclude the paper in Sec. VI with a brief summary and highlights of the primary results of the paper and their consequences for BEC dynamics, confinement, and growth.

## II. STATIONARY SOLUTIONS

The NLS (1) with  $V(x) = 0$  is an integrable equation and many explicit solutions are known, corresponding to various boundary conditions. A good description is found in [18]. If  $V(x) \neq 0$ , NLS is not integrable. In this case, only small classes of explicit solutions can most likely be obtained. Our choice of potential (2) is motivated by the form of the stationary solution of the NLS with  $V(x) = 0$ . An overview of these stationary solutions and their properties is found in [7]. For now, we restrict our solutions to stationary solutions of (1), *i.e.*, solutions whose time-dependence is restricted to

$$\psi(x, t) = \exp(-i\omega t + i\theta(x)) r(x). \quad (3)$$

If  $\theta_x \equiv 0$ , then the solution is referred to as having trivial phase. In this case we always let  $\theta(x) = 0$ . Substitution of the ansatz (3) in (1) and dividing out the exponential factor results in two equations: one from the real part and one from the imaginary part. The second equation can be integrated and gives

$$\theta(x, t) = c \int_0^x \frac{dx'}{r^2(x')}, \quad (4)$$

where  $c$  is a constant of integration. Notice that  $\theta(x)$  is a monotonous function of  $x$ . Substitution of this result in the remaining equation gives

$$\omega r^4(x) = \frac{c}{2} - \frac{r^3(x)r''(x)}{2} + r^6(x) - V_0 \text{sn}^2(x, k)r^4(x). \quad (5)$$

The following subsections describe two classes of solutions of this equation.

### Type A

#### 1. Derivation

For these solutions,  $r^2(x)$  is a quadratic function of  $\text{sn}(x, k)$ :

$$r^2(x) = A \text{sn}^2(x, k) + B. \quad (6)$$

Substitution of this ansatz in (5) and equating the coefficients of equal powers of  $\text{sn}(x, k)$  results in relations among the solution parameters  $\omega, c, A$  and  $B$  and the equation parameters  $V_0$  and  $k$ . These are

$$\omega = \frac{1}{2} \left( 1 + k^2 + 3B - \frac{BV_0}{V_0 + k^2} \right), \quad (7a)$$

$$c^2 = B \left( 1 + \frac{B}{V_0 + k^2} \right) (V_0 + k^2 + Bk^2), \quad (7b)$$

$$A = V_0 + k^2. \quad (7c)$$

Thus, for a given potential  $V(x)$ , this solution class has one free parameter  $B$ , playing the role of a constant background level or DC offset. The freedom in choosing the potential gives a total of three free parameters:  $V_0, k$  and  $B$ .

The requirements that both  $r^2(x)$  and  $c^2$  are positive, imposes conditions on the domain of these parameters. One needs

$$V_0 \geq -k^2, \quad B \geq 0, \quad \text{or} \quad (8a)$$

$$V_0 \leq -k^2, \quad -(V_0 + k^2) \leq B \leq -\left(1 + \frac{V_0}{k^2}\right). \quad (8b)$$

The region of validity of these solutions is displayed in Fig. 2.

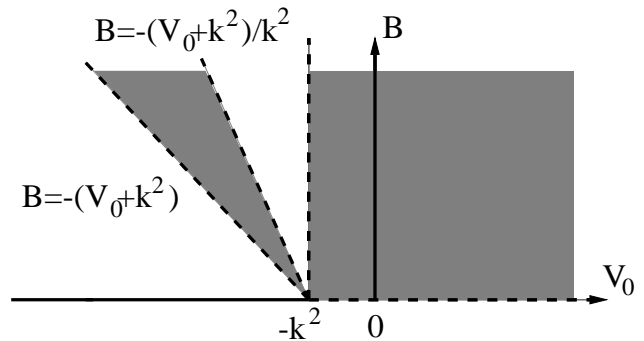


FIG. 2. The region of validity of the solutions of Type A is displayed shaded for a fixed value of  $k$ . The edges of these regions correspond to various trivial phase solutions.

For generic values of  $V_0$ ,  $k$  and  $B$ , the above equations give rise to solutions of Eqn. (1) which are not periodic in  $x$ :  $r(x)$  is periodic with period  $2K(k)$ , whereas  $\exp(i\theta(x))$  is periodic with period  $T = \theta^{-1}(2\pi)$ . In general these two periods  $2K(k)$  and  $T$  are not commensurable. Requiring periodic solutions results in another condition, namely  $2K(k)/T = p/q$ , for two positive integers  $p$  and  $q$ . The most convenient way to express this phase quantization condition is to assume the potential (*i.e.*,  $V_0$  and  $k$ ) is given, and to look for which values of  $B$  the quantization condition is satisfied. Introducing  $\beta = B/(V_0 + k^2)$ , we get

$$\pm \frac{\sqrt{\beta(1+\beta)(1+k^2\beta)}}{\pi} \int_0^{K(k)} \frac{dx}{\text{sn}(x,k)^2 + \beta} = \frac{p}{q}. \quad (9)$$

This equation is solved for  $\beta$ , after which  $B = \beta(V_0 + k^2)$ . For numerical simulations, the number of periods of the potential is set. This determines  $q$ , limiting the number of solutions of (9). If one wants solutions that have the same period as the potential, then  $p/q = 1$ .

Note that solutions of Type A reduce to stationary solutions of (1) and (2) with  $V_0 = 0$ . Furthermore, all stationary solutions of the integrable equation are obtained as limits of solutions of Type A.

## 2. Limits and Properties

The properties of these solutions are best understood by considering their various limit cases.

**The trivial phase case:** The solutions of Type A have trivial phase when  $c = 0$ . Since  $c^2$  has three factors which are linear in  $B$  (see (7)), there are three choices of  $B$  that make this happen:  $B = 0$ ,  $B = -(V_0 + k^2)$  and  $B = -(V_0 + k^2)/k^2$ . These possibilities are three of the four boundary lines of the region of validity in Fig. 2. Note that the remaining boundary line ( $V_0 = -k^2$ ) corresponds to  $r^2(x) = B$ , which gives rise to a plane wave solution. Using identities on Jacobian elliptic functions [15], one finds that the three other boundary lines give rise to simplified solution forms:  $B = 0$  gives

$$r(x) = \sqrt{V_0 + k^2} \text{sn}(x, k), \quad \omega = \frac{1 + k^2}{2}. \quad (10)$$

$B = -(V_0 + k^2)$  gives

$$r(x) = \sqrt{-(V_0 + k^2)} \text{cn}(x, k), \quad \omega = \frac{1}{2} - V_0 - k^2, \quad (11)$$

where  $\text{cn}(x, k)$  denotes the Jacobian elliptic cosine function. Lastly,  $B = -(V_0 + k^2)/k^2$  gives

$$r(x) = \frac{\sqrt{-(V_0 + k^2)}}{k} \text{dn}(x, k), \quad \omega = -1 - \frac{V_0}{k^2} + \frac{k^2}{2}, \quad (12)$$

where  $\text{dn}(x, k)$  denotes the third Jacobian elliptic function. Eqn (10) is valid for  $V_0 \geq -k^2$ , whereas the other two equations (11) and (12) are valid for  $V_0 \leq -k^2$ . The amplitude of these solutions  $A$  as a function of potential strength  $V_0$  is shown in Fig. 3.

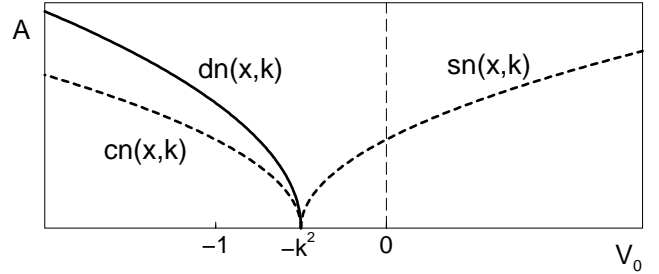


FIG. 3. The amplitude of the trivial phase solutions of Type A vs. the potential strength  $V_0$ .

Both  $\text{cn}(x, k)$  and  $\text{sn}(x, k)$  have zero average as functions of  $x$  and lie in  $[-1, 1]$ . On the other hand,  $\text{dn}(x, k)$  has nonzero average. It's range is  $[\sqrt{1 - k^2}, 1]$ . Furthermore,  $\text{cn}(x, k)$  and  $\text{sn}(x, k)$  are periodic in  $x$  with period  $4K(k)$ , whereas  $\text{dn}(x, k)$  is periodic with period  $2K(k)$ . These properties matter greatly for the stability analysis, as will be seen in Section 3. Some solutions with trivial phase are shown in Fig. 4.

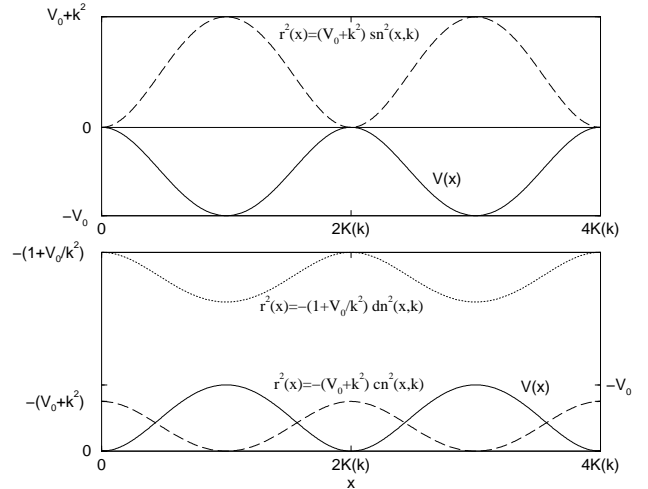


FIG. 4. Trivial phase solutions for  $k = 0.5$ .  $V(x)$  is indicated with a solid line. For the top figure  $V_0 = 1$ . For the bottom figure  $V_0 = -1$ .

**The trigonometric limit:** In the limit  $k \rightarrow 0$ , the elliptic functions reduce to trigonometric functions. The potential (2) becomes  $V(x) = -V_0 \sin^2(x) = (V_0/2) \cos(2x) - V_0/2$ . Then

$$r^2(x) = V_0 \sin^2(x) + B, \quad \omega = \frac{1}{2} + B. \quad (13)$$

In this case, the phase integral (4) results in

$$\tan(\theta(x)) = \pm \sqrt{1 + V_0/B} \tan(x). \quad (14)$$

Note that this formula guarantees that the resulting solution is periodic with the same period as the potential, so no phase quantization is required. In the trigonometric limit, the wedge between the two regions of validity in Fig. 2 disappears. This is no surprise, as in this limit,  $\text{dn}(x, k) \rightarrow 1$ , and the third trivial phase solution reduces to a plane wave solution. The cornerpoint of the region of validity also moves to the origin.

Some trigonometric solutions are displayed in Fig. 5.

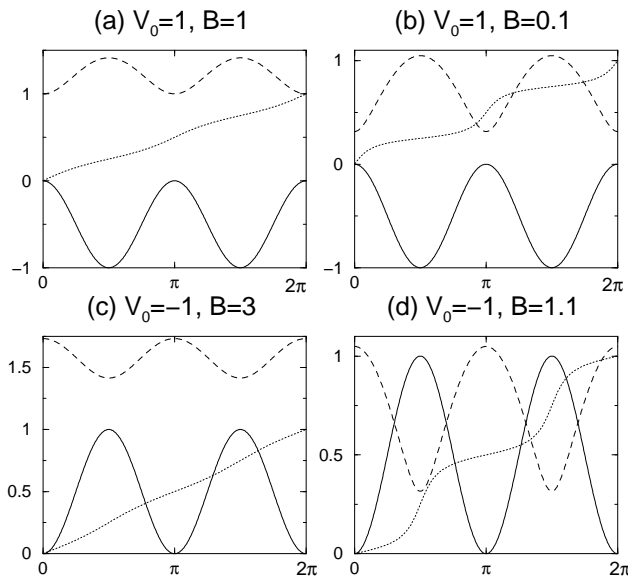


FIG. 5. Some trigonometric solutions. For all these figures, the solid line denotes  $V(x)$ , the dashed line is  $r(x)$  and the dotted line is  $\theta(x)/(2\pi)$ . Notice that  $\theta(x)$  becomes piecewise constant, as  $B$  approaches the boundary of the region of validity. Far away from this boundary,  $\theta(x)$  is essentially linear.

**The solitary wave limit** As  $k \rightarrow 1$ , the elliptic functions reduce to hyperbolic functions. Specifically,  $\text{sn}(x, k) \rightarrow \tanh(x)$ , as  $k \rightarrow 1$ . Hence in this limit, the potential has only a single well or a single peak. Then  $V_0 < 0$  gives rise to a repulsive potential, whereas  $V_0 > 0$  gives rise to an attractive potential:  $V(x) = -V_0 \tanh^2(x)$ . In this case the phase  $\theta(x)$  (4) can be calculated explicitly:

$$r^2(x) = (V_0 + 1) \tanh^2(x) + B, \quad (15a)$$

$$c^2 = B(V_0 + 1 + B)^2 / (V_0 + 1), \quad (15b)$$

$$\theta(x) = c(V_0 + 1 + B)x - c(V_0 + 1) \tanh(x). \quad (15c)$$

The region of validity now consists of  $V_0 > -1, B > 0$  or  $B = -(V_0 + 1) > 0$ . In the first region  $r^2(x) = \sqrt{(V_0 + 1) \tanh^2(x) + B}$ , and the solution is a stationary solitary wave of depression on a positive background. This solution is a deformation of the dark (more precisely: gray) soliton solution of the NLS equation with repulsive nonlinearity. Note that these solutions can exist with an attractive potential, as long as  $-1 < V_0 < 0$ . Two solutions with repulsive potential are illustrated in Fig. 6a-b. The second region is a half line, and  $\theta(x) = 0$  on this half line. Then  $r(x) = \sqrt{-(V_0 + 1)} \text{sech}(x)$ . This solution represents a stationary elevated solitary wave. It is reminiscent of the bright soliton solution of the NLS equation with attractive nonlinearity. This solution is shown in Fig. 6c. A surprising consequence of considering NLS (1) is that the potential strength  $V_0$  acts as a switch between the equation with repulsive and attractive nonlinearity, as illustrated by these solitary wave solutions.

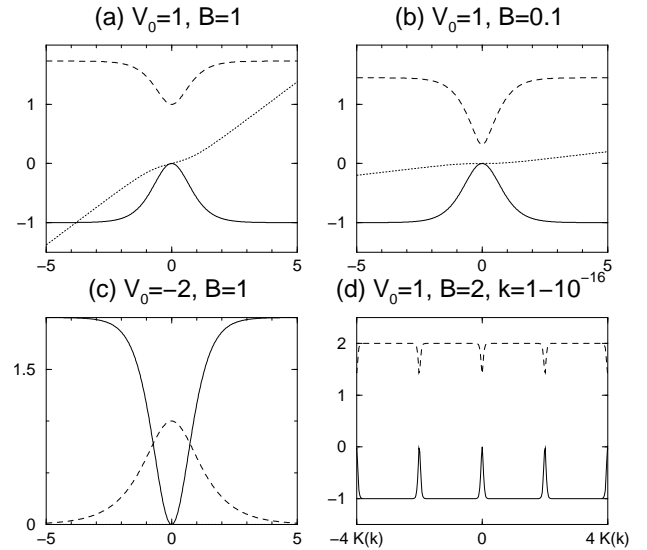


FIG. 6. Solutions with  $k=1$  (a,b,c) or  $k \rightarrow 1$  (d). For figures a,b and c the solid line denotes  $V(x)$ , the dashed line is  $r(x)$  and the dotted line is  $\theta(x)/20$ . In (d), a value of  $k = 1 - 10^{-16}$  was used. This is better for illustrative purposes than letting  $k = 1$ . The solid line is  $\hat{V}(x)$ , the dashed line is  $\hat{r}(x)$  and the dotted line is  $\hat{\theta}(x)/(2\pi)$ .

Understanding the solitary wave limit facilitates the understanding of what happens when  $k$  is very close to one. In this case the solutions of Type A reduce to a periodic train of solitons with exponentially small interactions. This is illustrated in Figure 6d.

## Type B

### 1. Derivation

For these solutions,  $r^2(x)$  is linear in  $\text{cn}(x, k)$  or  $\text{dn}(x, k)$ . First we discuss the solution with  $\text{cn}(x, k)$ . The quantities associated with this solution will be denoted with a subindex 1. The quantities associated with the  $\text{dn}(x, k)$  solution receive a subindex 2.

Substituting

$$r_1^2(x) = a_1 \text{cn}(x, k) + b_1, \quad (16)$$

in (5) and equating different powers of  $\text{cn}(x, k)$  as before gives the following relations:

$$V_0 = -\frac{3}{8}k^2, \quad (17a)$$

$$\omega_1 = \frac{1}{8}(1+k^2) + \frac{6a_1^2}{k^2}, \quad (17b)$$

$$c_1^2 = \frac{a_1^2}{4k^6}(4a_1+k^2)(4a_1-k^2)(16a_1^2+k^2-k^4) \quad (17c)$$

$$b_1 = \frac{4a_1^2}{k^2}. \quad (17d)$$

The class of potentials (2) is restricted by the first of these relations. Now the potential strength  $V_0$  is limited to a narrow range:  $-3/8 \leq V_0 \leq 0$ . The solution class now depends on one free amplitude parameter  $a_1$  and the free equation parameter  $k$ .

The region of validity of this solution is, as before, determined by the requirements  $c_1^2 \geq 0$  and  $r_1^2(x) \geq 0$ :

$$|a_1| \geq \frac{k^2}{4}. \quad (18)$$

The period of  $r_1(x)$  is twice the period of the potential. Requiring periodicity in  $x$  of this first solution of Type B gives

$$\pm \frac{\sqrt{(\beta_1^2 - k^2)(\beta_1^2 + 1 - k^2)}}{4\pi} \int_0^{2K(k)} \frac{dx}{4\beta_1 + k \text{cn}(x, k)} = \frac{p}{q}. \quad (19)$$

For given  $k$  and integers  $p, q$ , this equation is solved for  $\beta_1$ , from which  $a_1 = \beta_1 k/4$ .

Next we discuss the solution with  $\text{dn}(x, k)$ . Substituting

$$r_2^2(x) = a_2 \text{dn}(x, k) + b_2, \quad (20)$$

in (5) and equating different powers of  $\text{dn}(x, k)$  imposes the following constraints on the parameters:

$$V_0 = -\frac{3}{8}k^2, \quad (21a)$$

$$\omega_2 = \frac{1}{8}(1+k^2) + 6a_2^2, \quad (21b)$$

$$c_2^2 = \frac{a_2^2}{4}(4a_2+1)(4a_2-1)(16a_2^2+k^2-1), \quad (21c)$$

$$b_2 = 4a_2^2. \quad (21d)$$

The class of potentials (2) is restricted as for the previous solution by the first of these relations. The solution class again depends on one free amplitude parameter  $a_2$  and the free equation parameter  $k$ .

The region of validity of this solution is once more determined by the requirements  $c_2^2 \geq 0$  and  $r_2^2(x) \geq 0$ :

$$|a_2| \geq \frac{1}{4} \quad \text{or} \quad 0 \leq a_2 \leq \frac{\sqrt{1-k^2}}{4}. \quad (22)$$

The period of  $r_2(x)$  is equal to the period of the potential. Requiring periodicity in  $x$  of this second solution of Type B gives

$$\pm \frac{\sqrt{(16a_2^2-1)(16a_2^2+k^2-1)}}{\pi} \int_0^{K(k)} \frac{dx}{4a_2 + \text{dn}(x, k)} = \frac{p}{q}. \quad (23)$$

For given  $k$  and integers  $p, q$ , this equation needs to be solved for  $a_2$ .

In contrast to solutions of Type A, solutions of Type B do not have a nontrivial trigonometric limit. In fact, for solutions of Type B, this limit is identical to the limit in which the potential strength  $V_0 = -3k^2/8$  approaches zero. Thus it is clear that the solutions of Type B have no analogue in the integrable nonlinear Schrödinger equation. However, other interesting limits do exist.

### 2. Limits and Properties

**The trivial phase case:** Trivial phase corresponds to  $c = 0$ . This occurs precisely at the boundaries of the regions of validity. For the first solution of Type B, there are two possibilities:  $a_1 = k^2/4$  or  $a_1 = -k^2/4$ . By replacing  $x$  by  $x + 2K(k)$ , one sees that these two possibilities are completely equivalent, so only the first one needs to be considered:

$$r_1^2(x) = \frac{k^2}{4}(1 + \text{cn}(x, k)), \quad \omega_1 = \frac{1}{8} + \frac{k^2}{2}. \quad (24)$$

For the second solution, there are four possibilities:  $a_2 = 1/4$ ,  $a_2 = -1/4$ ,  $a_2 = 0$  and  $a_2 = \sqrt{1-k^2}/4$ . The third one of these results in a zero solution. The others give interesting trivial phase solutions. For  $a_2 = 1/4$ ,

$$r_2^2(x) = \frac{1}{4}(1 + \text{dn}(x, k)), \quad \omega_2 = \frac{1}{2} + \frac{k^2}{8}. \quad (25)$$

Next,  $a_2 = -1/4$  gives

$$r_2^2(x) = \frac{1}{4}(1 - \text{dn}(x, k)), \quad \omega_2 = \frac{1}{2} + \frac{k^2}{8}. \quad (26)$$

Lastly, for  $a_2 = \sqrt{1 - k^2}/4$ ,

$$r_2^2(x) = \frac{\sqrt{1 - k^2}}{4} (\text{dn}(x, k) + \sqrt{1 - k^2}), \quad \omega_2 = \frac{1}{2} - \frac{k^2}{2}. \quad (27)$$

These solutions are shown in Fig. 7.

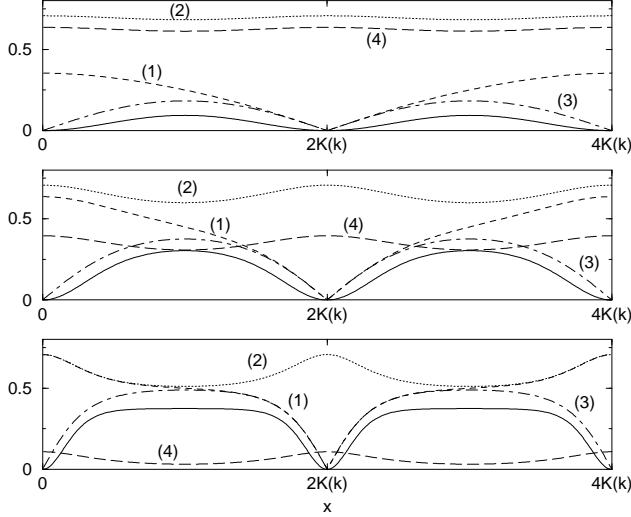


FIG. 7. Solutions of Type B with trivial phase. The figures correspond to, from top to bottom,  $k = 0.5$ ,  $k = 0.9$  and  $k = 0.999$ . The potential is indicated in a solid line. The other curves are: (1)  $|r_1(x)|$  with  $a_2 = k^2/4$ , (2)  $r_2(x)$  with  $a_2 = 1/4$ , (3)  $|r_2(x)|$  with  $a_2 = -1/4$  and (4)  $r_2(x)$  with  $a_2 = \sqrt{1 - k^2}/4$ .

**The solitary wave limit:** In this limit  $V_0 = -3/8$  and the potential is  $V(x) = 3 \tanh(x)^2/8$ . Since both  $\text{cn}(x, k) \rightarrow \text{sech}(x)$  and  $\text{dn}(x, k) \rightarrow \text{sech}(x)$  as  $k \rightarrow 1$ ,  $r_1(x) = r_2(x)$  in the solitary wave limit. Their ranges of validity also share the same limit:  $|a| \geq 1/4$ , with  $a = a_1 = a_2$ . The phase can be calculated explicitly and the solitary wave solution of Type B is

$$r^2(x) = 4a^2 + a \text{sech}(x), \quad (28a)$$

$$\theta(x) = \pm \left( \frac{x\sqrt{16a^2 - 1}}{2} + \arctan \left( \sqrt{\frac{4a - 1}{4a + 1}} \tanh \frac{x}{2} \right) \right). \quad (28b)$$

The region of validity consists of two separated regions:  $a \geq 1/4$  and  $a \leq -1/4$ . In the first region, the solution is a stationary elevated solitary wave, on a constant background  $4a^2$ . In the second region  $a \leq -1/4$  and the solution is a stationary solitary wave of depression, on a constant background  $4a^2$ . These solitary wave solutions are illustrated in Fig. 8

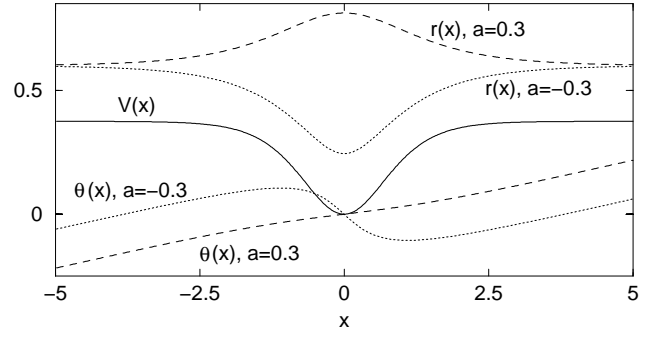


FIG. 8. Solitary wave solutions of Type B. The potential is indicated with a solid line. The dashed line solution corresponds to  $a = 0.3$ , the dotted line to  $a = -0.3$ .

As for the solutions of type A, the solitary wave limit gives an idea of the behavior of the solution for values of  $k$  close to one, where the solution behaves as a periodic array of solitons with exponentially small interactions.

**A note on the linear limit:** The linear Schrödinger equation is obtained when the potential dominates the nonlinear term.

Unfortunately, none of the solutions of Type A have a nontrivial (*i.e.*, nonzero) linear limit. This is seen as follows: the linear limit requires the potential to dominate the nonlinear term. However, a large value for the potential strength  $V_0$  implies a large value for  $A = V_0 + k^2$ , which implies a large maximal value for  $r(x)$ . Hence, the nonlinear term cannot be ignored.

However, there are solutions of Type B for which the potential strength dominates the solution strength, as illustrated in the bottom figure of Fig. 7: if  $0 \leq a_2 \leq \sqrt{1 - k^2}/4$  and  $k$  is close to 1, the potential approaches  $V(x) = 3 \text{sn}^2(x, k)/8 \approx 3 \tanh^2(x)/8$ , whereas  $r_2^2(x) = \epsilon \text{dn}(x, k) + \epsilon^2 \approx \epsilon \text{sech}(x) + \epsilon^2$ , where  $0 \leq \epsilon \leq \sqrt{1 - k^2}/4$ .

### III. STABILITY

We have found a large number of new solutions to the governing Eqs. (1) and (2). However, only solutions that are stable can be observed in experiments. In this section, we consider the stability of the different solutions. Both analytical and numerical results are presented for the solutions with trivial phase. In contrast, only numerical results are presented for the nontrivial phase cases.

The linear stability of solutions of the form (3) of the NLS equation (1) is investigated. To do so, the exact solutions are perturbed by considering:

$$\psi = (r(x) + \epsilon \phi(x, t)) e^{i(\theta(x) - \omega t)} \quad (29)$$

where  $\epsilon \ll 1$  is a small parameter. Collecting terms at  $O(\epsilon)$  the linearized equation is obtained. Its real and imaginary parts are  $\mathbf{U} = (U_1, U_2)^t = (\text{Re}[\phi], \text{Im}[\phi])^t$ :

$$\mathbf{U}_t = JLU = J \begin{pmatrix} L_+ & S \\ -S & L_- \end{pmatrix} \mathbf{U}, \quad (30)$$

where

$$L_+ = -\frac{1}{2} \left( \partial_x^2 - \frac{c^2}{r^4} \right) + 3r(x)^2 + V(x) - \omega, \quad (31a)$$

$$L_- = -\frac{1}{2} \left( \partial_x^2 - \frac{c^2}{r^4} \right) + r(x)^2 + V(x) - \omega, \quad (31b)$$

$$S = \frac{c}{r(x)} \partial_x \frac{1}{r(x)}, \quad (31c)$$

and  $J = \begin{pmatrix} 0 & -1 \\ 1 & 0 \end{pmatrix}$  is a skew-symmetric matrix. The operator  $L$  is Hermitian as are  $L_+$  and  $L_-$  while  $S$  is anti-Hermitian. Considering solutions of the form  $\mathbf{U}(x, t) = \hat{\mathbf{U}}(x) \exp(\lambda t)$  gives the eigenvalue problem

$$\mathcal{L}\hat{\mathbf{U}} = \lambda\hat{\mathbf{U}}, \quad (32)$$

where  $\mathcal{L} = JL$  and  $\lambda$  is complex. If all  $\lambda$  are imaginary, then linear stability is established. In contrast, if there is at least one eigenvalue with a positive real part, then instability results. Using the phase invariance  $\psi \mapsto e^{i\gamma}\psi$  of Eq. (1), Noether's theorem [19] gives

$$\mathcal{L} \begin{pmatrix} 0 \\ r(x) \end{pmatrix} = 0, \quad (33)$$

which implies that  $L_- r(x) = 0$ . Thus  $\lambda = 0$  is in the spectrum of  $L_-$ . For general solutions of the form (3), determining the spectrum of the associated linearized eigenvalue problem (30) is beyond the scope of current methods. However, some cases of trivial phase solutions ( $c = 0$ ) are amenable to analysis.

From classical results [19] it follows that the spectra of the Hermitian operators  $L_{\pm}$  are on the real line in an interval  $\lambda \in [\lambda_{\pm}, \infty)$ . Here  $\lambda_{\pm}$  denote the left-most points of the spectra of  $L_{\pm}$  respectively. They are determined by

$$\lambda_{\pm} = \inf_{\|\phi\|=1} \langle \phi | L_{\pm} | \phi \rangle, \quad (34)$$

where  $\|\phi\|^2 = \langle \phi | \phi \rangle$ . The associated eigenfunctions are the ground states of the operator  $L_{\pm}$  respectively. From the relation  $L_+ = L_- + 2r^2$  it follows that  $\lambda_+ > \lambda_-$ . Also  $\lambda_- \leq 0$  since  $\lambda = 0$  is an eigenvalue of  $L_-$ .

For  $L_+ > 0$  the Hermitian operator  $H = L_+^{\frac{1}{2}} L_- L_+^{\frac{1}{2}}$  can be constructed. Note that if  $L_+$  is Hermitian and strictly positive it has a positive Hermitian square root,  $L_+^{\frac{1}{2}}$ , which is conveniently obtained from the spectral representation [19]. The eigenvalue problem for  $\mathcal{L}$  in Eq. (32) is then equivalent to

$$(H + \lambda^2)U_1 = 0. \quad (35)$$

Denote the left-most point of the spectrum of  $H$  by  $\mu_0$ . If  $\mu_0 \geq 0$  then  $\lambda^2 < 0$  and the eigenvalues of  $\mathcal{L}$  are imaginary and linear stability results. In contrast, if  $\mu_0 < 0$

then  $\lambda^2 > 0$  and  $\mathcal{L}$  has at least one pair of real eigenvalues with opposite sign. This shows the existence of a growing mode leading to instability of the solution.

Three distinct cases are possible for linear stability

- If  $r(x) > 0$  then Eq. (33) implies  $r(x)$  is the ground state of  $L_-$  so that  $\lambda_- = 0$  [19] and  $\lambda_+ > 0$ . Thus the solution (3) is linearly stable.
- If  $r(x)$  has a zero, it is no longer the ground state [19] and  $\lambda_- < 0$ . Thus there exists a  $\psi_0$  such that  $\langle \psi_0 | L_- | \psi_0 \rangle < 0$ . If in addition  $\lambda_+ > 0$ , then we can construct  $\phi = L_+^{-\frac{1}{2}} \psi_0 / \|L_+^{-\frac{1}{2}} \psi_0\|$  which gives  $\langle \phi | H | \phi \rangle < 0$ . Hence  $\mu_0 < 0$  and  $\mathcal{L}$  has positive, real eigenvalues so that the solution (3) is linearly unstable.
- For  $\lambda_-$  and  $\lambda_+$  both negative the situation is indefinite and our methods are insufficient to determine linear stability or instability.

In what follows, these results are applied to the Type A and B trivial phase solutions constructed in the preceding section. Specifically, we construct the operators  $L_-$  and  $L_+$  for each solution, which allows us to use one of the above criteria for determining stability or instability.

## A. trivial phase: Type A

### 1. $cn(x, k)$

The stability analysis of the  $cn(x, k)$  solution requires the study of the operator  $L_+$  which takes the form

$$L_+ = -\frac{1}{2} \partial_x^2 - (2V_0 + 3k^2) \text{cn}^2(x, k) + k^2 - \frac{1}{2} \quad (36)$$

with  $V_0 < -k^2$ . If we only consider the parameter region  $V_0 < -k^2 - 1/4$ , then  $L_+ > 0$ . The operator  $L_-$  is

$$L_- = -\frac{1}{2} \partial_x^2 - k^2 \text{cn}^2(x, k) + k^2 - \frac{1}{2}, \quad (37)$$

which is independent of  $V_0$  and satisfies  $L_- \text{dn}(x, k) = -(1 - k^2/2) \text{dn}(x, k)$ . Since  $\text{dn}(x, k) > 0$  we have  $\lambda_- = -(1 - k^2/2) < 0$  so that by the arguments of the previous section the  $cn(x, k)$  wave is unstable for these parameter values. This result leaves the stability of the  $cn(x, k)$  solution undetermined for the parameter region  $-k^2 - 1/4 < V_0 < -k^2$ . However, numerical simulations show these solutions to be unstable as well.

To illustrate this instability, we display in Figure 9 the evolution of a  $cn(x, k)$  solution over the time interval  $t \in [0, 40]$  and for  $V_0 = -1.0$  and  $k = 0.5$ . The computational run was for twelve spatial periods but only four

periods are shown to better illustrate the instability. The solution goes quickly unstable with the instability generated near the first wavenumber. This is as predicted analytically. It is illustrated in the evolution of the Fourier mode spectrum in Fig. 10. Here a close-up of the Fourier modes near wavenumber unity is shown. The close-up shows definitively that the instability indeed occurs near the unstable modes predicted from the linear stability analysis.

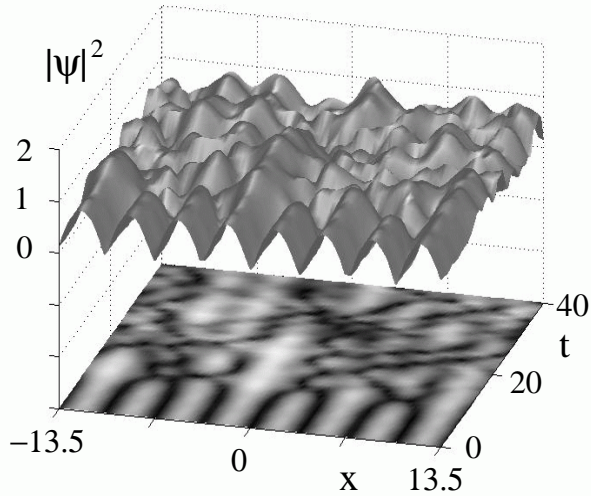


FIG. 9. Unstable evolution of a Type A  $\text{cn}(x, k)$  solution given by Eq. (11) over 40 time units with  $k = 0.5$  and  $V_0 = -1.0$ . Only four of the twelve spatial periods of the computational run are displayed to illustrate the resulting instability more clearly.

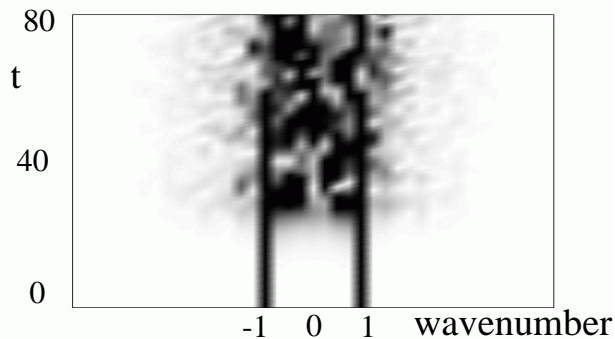


FIG. 10. Fourier spectrum evolution of the Type A  $\text{cn}(x, k)$  branch of solutions given by Eq. (11) over 40 time units with  $k = 0.5$  and  $V_0 = -1.0$ . The modal evolution shows the band of unstable modes which result from starting with the unstable  $\text{cn}(x, k)$  solution. Note that the instability is generated near a wavenumber of unity as predicted by the linear stability analysis.

## 2. $\text{sn}(x, k)$

From numerical results, the  $\text{sn}(x, k)$  solutions given by Eq. (10) are also unstable. However, in contrast to the  $\text{cn}(x, k)$  solutions, the linear stability analysis is indefinite since both  $\lambda_+$  and  $\lambda_-$  are negative. Similar to the  $\text{cn}(x, k)$  solution, the  $\text{sn}(x, k)$  solution goes unstable quickly with the instability generated near the first wavenumber. The dynamics of the unstable evolution is qualitatively the same as in Fig. 9. The Fourier spectrum closely resembles Fig. 10. This unstable behavior is not surprising, since the  $\text{sn}(x, k)$  solutions are closely related to the  $\text{cn}(x, k)$  with only a half period shift of the solution. Combined with a change in sign of the potential, the character of the solutions is very similar.

## 3. $\text{dn}(x, k)$

From the previously established results, linear stability for the  $\text{dn}(x, k)$  solutions follows immediately since  $r(x) > 0$ , because  $\text{dn}(x, k)$  has no zeros. Thus in contrast to the  $\text{cn}(x, k)$  and  $\text{sn}(x, k)$  solutions, the  $\text{dn}(x, k)$  solutions given by Eq. (12) are linearly stable. Figure 11 displays the evolution of a  $\text{dn}(x, k)$  solution over the time interval  $t \in [0, 80]$  and for  $V_0 = -1.0$  and  $k = 0.5$ . The computational run was for twelve spatial periods but only four periods are depicted for clarity. Although noise was added in to the initial data, the solution shape persists and the solution is stable, as predicted analytically. For this case, the Fourier mode spectra is made up primarily of three modes: the zero mode which determines the offset, and two other modes which determine the oscillation frequency and strength of the  $\text{dn}(x, k)$  solution. Even with large perturbations, this solution persists. This indicates that the offset of a solution is important for the stability of a solution. This observation is reconfirmed for other stable solutions below.

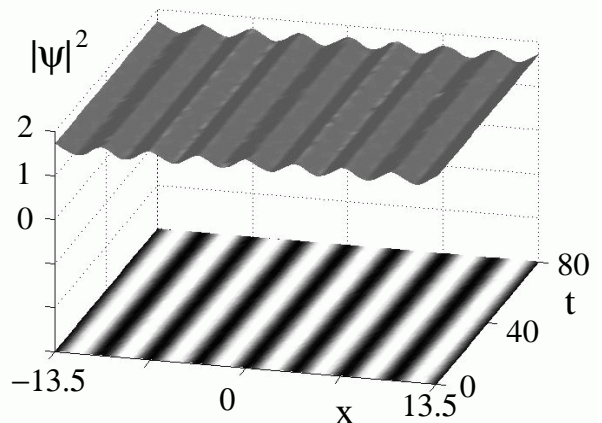


FIG. 11. Stable evolution of the Type A  $\text{dn}(x, k)$  solutions given by Eq. (12) over 80 time units with  $k = 0.5$  and  $V_0 = -1.0$ . Only four of the twelve spatial periods of the computational run are depicted for clarity.

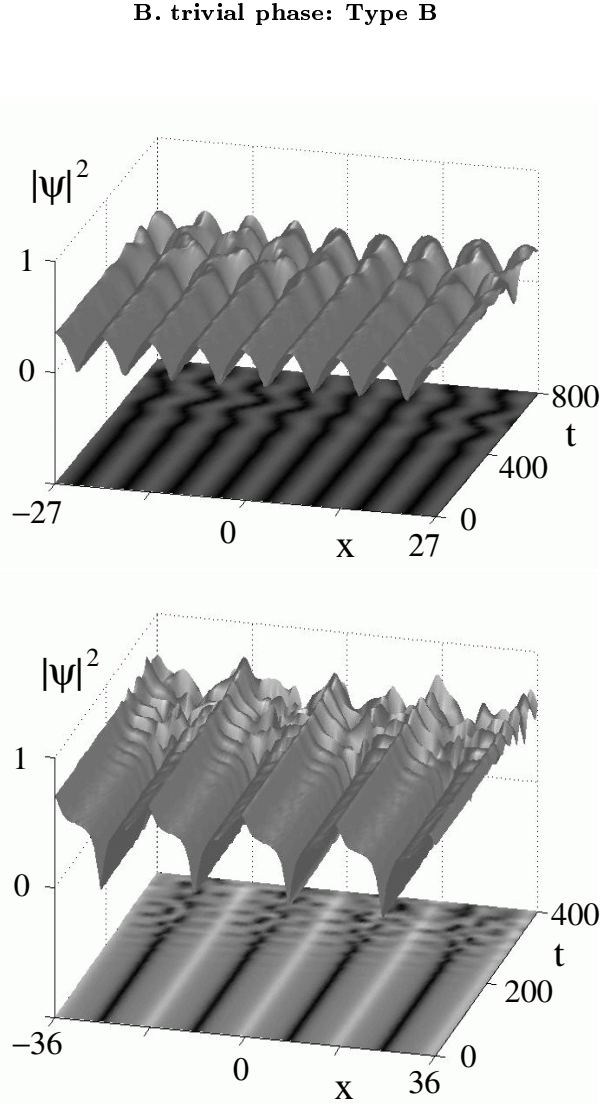


FIG. 12. Unstable evolution of the Type B  $\text{cn}(x, k)$  solutions given by Eq. (24) for  $k = 0.5$  (top panel) and  $k = 0.999$  (bottom panel) for  $a_1 = k^2/4$  and  $V_0 = -3k^3/8$ . Only four of the twelve spatial periods of the computational run are displayed to illustrate the resulting instability more clearly.

### 1. $\text{cn}(x, k)$

The Type B trivial phase solution is obtained for  $a_1 = \pm k^2/4$  and corresponding amplitude  $|r(x)| = (k/2)\sqrt{1 + \text{cn}(x, k)}$ . The solution  $r(x)$  is not strictly positive. The operator  $L_+$  is

$$L_+ = -\frac{1}{2}\partial_x^2 + \frac{k^2}{4} - \frac{1}{8} + \frac{3}{8}k^2 \text{sn}^2 + 3a_1 \text{cn}. \quad (38)$$

Thus we find that for  $k \rightarrow 0$ ,  $\lambda_+ < 0$  and the situation is indetermined. However, as  $k$  increases,  $\lambda_+$  increases and we arrive at the instability case  $\lambda_+ > 0$ .

Numerical simulations for the Type B  $\text{cn}(x, k)$  solutions given by Eq. (24) are illustrated in Fig. 12. This figure displays the evolution of the  $\text{cn}(x, k)$  branch of solution for  $k = 0.5$  (top panel) and  $k = 0.999$  (bottom panel) over the time interval  $t \in [0, 800]$  and  $t \in [0 : 400]$  respectively for  $V_0 = -3k^2/8$ . The computational run was for twelve spatial periods but only four periods are displayed to better illustrate the instability. For both  $k = 0.5$  and  $k = 0.999$  the solutions are unstable, but this instability manifests itself only after several hundred time units. Figure 13 shows the evolution of the Fourier spectrum for both these cases. For  $k = 0.5$ , the onset of instability occurs near wavenumber one as is the case of Type A solutions. After 800 time units, the Fourier modes have only just begun to spread, causing the solution to destabilize. For  $k = 0.999$ , the solution is composed of a much larger number of Fourier modes which destabilize much more quickly than the  $k = 0.5$  case. Here the instability is generated near wavenumber unity and its harmonics.

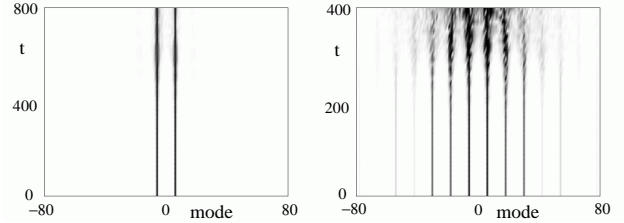


FIG. 13. Fourier spectrum evolution of the Type B  $\text{cn}(x, k)$  branch of solutions given by Eq. (11) for  $a_1 = k^2/4$  and corresponding to  $k = 0.5$  (left panel) and  $k = 0.999$  (right panel) of Fig 12. The evolution shows that the unstable band of modes are generated near wavenumber one and for  $k = 0.999$  near wavenumber one and its harmonics.

### 2. $\text{dn}(x, k)$

The trivial phase  $\text{dn}(x, k)$  solution requires  $c = 0$  which is achieved for  $a_2 = \pm 1/4$ ,  $a_2 = 0$ , or  $a_2 = \sqrt{1 - k^2}/4$ . Thus three distinct parameter regimes need to be considered. The relevant operators in this case are

$$L_+ = -\frac{1}{2}\partial_x^2 - \frac{k^2 + 1}{8} + 6a_2^2 + \frac{3}{8}k^2 \text{sn}^2 + 3a_2 \text{dn} \quad (39a)$$

$$L_- = -\frac{1}{2}\partial_x^2 - \frac{k^2 + 1}{8} - 2a_2^2 + \frac{3}{8}k^2 \text{sn}^2 + a_2 \text{dn} \quad (39b)$$

The case  $a_2 = 1/4$  gives  $L_-r(x) = 0$  with  $r(x) > 0$ . Hence from the linear stability criteria, these waves are

stable for all values of  $k$ . As with the  $a_2 = 1/4$  case, the regime where  $a_2 = \sqrt{1 - k^2}/4$  gives a solution  $r(x)$  which is strictly positive and is the ground state of  $L_-$ . Thus stability follows for all values of  $k$ . The last parameter regime, for which  $a_2 = -1/4$ , is indetermined since both  $\lambda_-$  and  $\lambda_+$  are negative and our linear stability analysis is inconclusive.

The analytic predictions are confirmed in Figs. 14–15. In Fig. 14 the evolution of a  $\text{dn}(x, k)$  solution is shown for  $a_2 = 1/4$  and  $k = 0.999$ . The computational run was for twelve spatial periods but only four periods are displayed for clarity. As predicted analytically, this parameter regime is stable for all  $k$  values. This simulation once again illustrates the importance of an offset for stabilizing the condensate [2]. In contrast to this stable evolution, the case  $a_2 = -1/4$  is unstable as illustrated in Fig. 15. The linear stability results in this case were indetermined. However, the numerical simulations conclusively show the evolution to be unstable for all  $k$  values. For this case, the offset of the solution is insufficient to stabilize the condensate. We note that for small values of  $k$ , the onset of instability occurs after a very long time. Higher values of  $k$  result in instabilities on a much faster time scale. Finally, we consider the parameter regime for which  $a_2 = \sqrt{1 - k^2}/4$ . In this case, the analytic predictions once again suggest stability for all  $k$  values. We do not illustrate this case in a figure since it is qualitatively very similar to Fig. 15. However, in contrast to the  $a_2 = 1/4$  case, for values of  $k$  close to one, there is a negligible amount of offset, distinguishing this stable case from previous ones. For these values of  $k$ , the solution has a small amplitude compared to the potential so that the behavior is essentially linear and stability is achieved because the condensate is trapped in the wells of the potential, as in ordinary quantum mechanics.

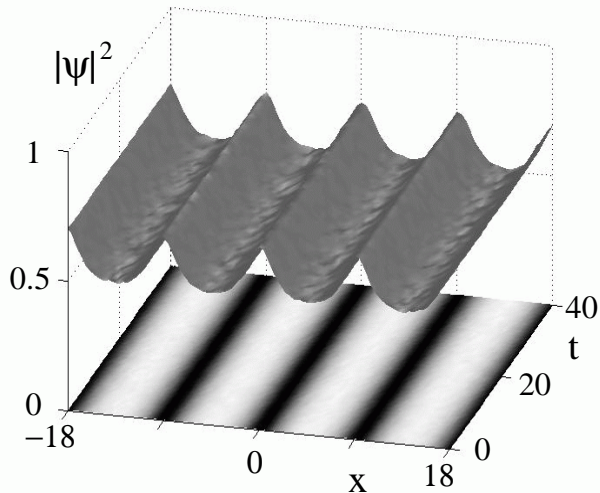


FIG. 14. Stable evolution of a Type B  $\text{dn}(x, k)$  solution given by Eq. (25) for  $k = 0.999$  and  $a_2 = 1/4$ . Only four of the twelve spatial periods of the computational run are shown to illustrate the resulting stable evolution more clearly.

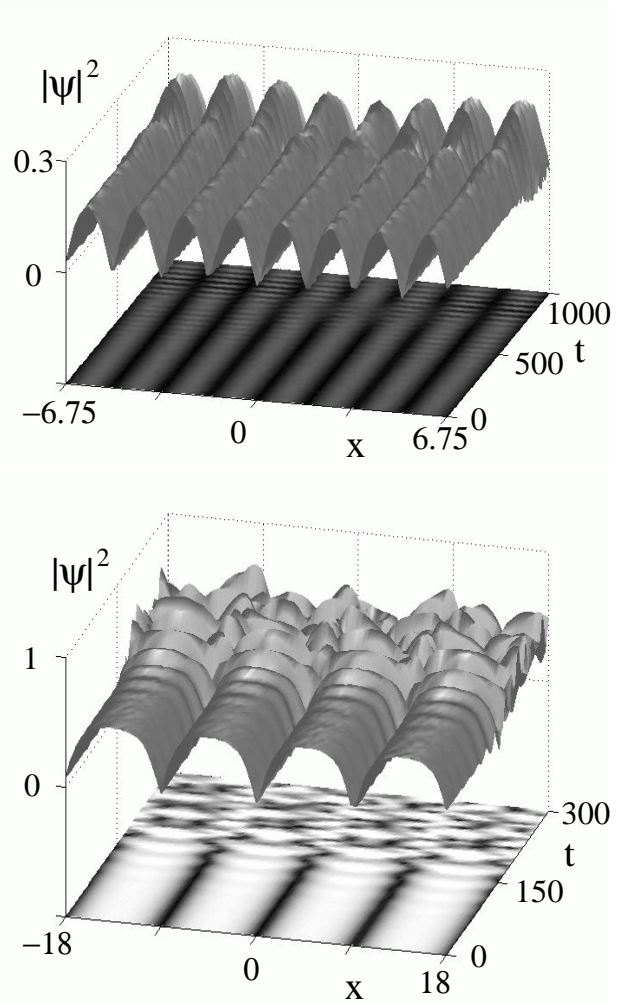


FIG. 15. Unstable evolution of a Type B  $\text{dn}(x, k)$  solution given by Eq. (26) for  $k = 0.5$  (top panel) and  $k = 0.999$  (bottom panel) given  $a_2 = -1/4$ . Only four of the twelve spatial periods of the computational run are shown to illustrate the resulting instability more clearly. In this case, there is no offset to stabilize the condensate.

### C. nontrivial phase: Type A

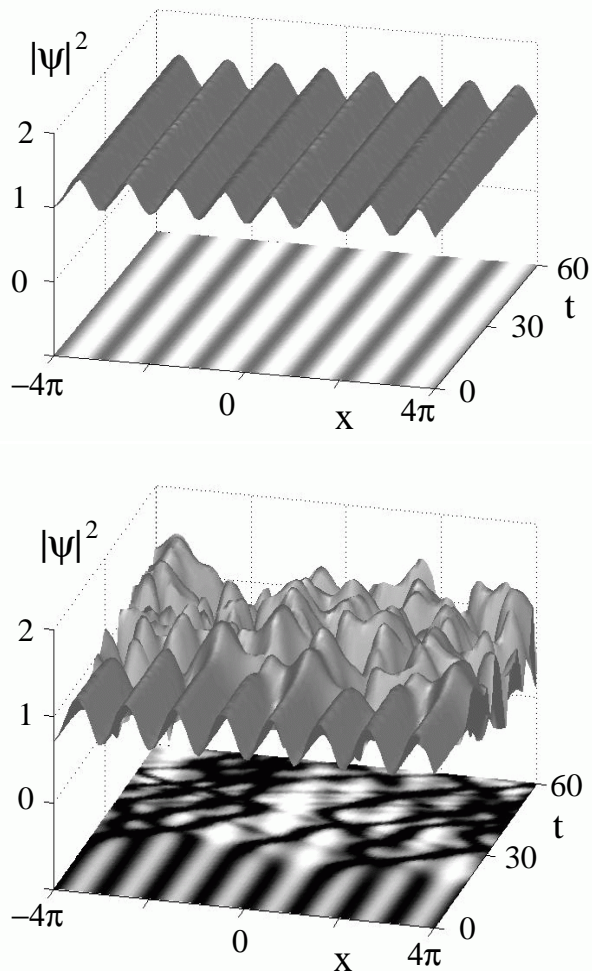


FIG. 16. Evolution of a nontrivial phase Type A solution with  $V_0 = 1.0$  and  $B = 1$  (top panel) and  $B = 1/2$  (bottom panel). For  $B$  sufficiently large, the offset provided is able to stabilize the condensate whereas for  $B$  below a critical threshold the condensate destabilizes as shown for  $B = 1/2$ .

As stated at the beginning of Section III, determining the linear stability for nontrivial phase solutions is not amenable to analysis since the associated eigenvalue problem is beyond the scope of current methods. This leads us to consider the stability of nontrivial phase solutions using numerical computations.

To begin, consider the trigonometric limit of the nontrivial phase solutions of Type A. These solutions are given by Eqs. (13) and (4). Figure 16 depicts the evolution of a pair of initial conditions with  $V_0 = 1.0$  and for which  $B = 1$  (top panel) and  $B = 1/2$  (bottom panel). Since  $B$  determines the offset of the condensate, these numerical results show directly the importance of this

offset for stability. For sufficiently large offset the solution resembles a  $\text{dn}(x, k)$ -like solution so that the solution remains close to the stationary solution for long times, which for our time scale is longer than the lifetime of typical trapped BECs [4]. In contrast, if the offset is too small, it is unable to stabilize the condensate.

### D. nontrivial phase: Type B

For Type B solutions, qualitatively nothing changes from the dynamics illustrated for the trivial phase case. In particular, numerical simulations can be performed using exact solutions which are constructed subject to the phase quantization condition given by either Eq. (19) or (23). A numerical shooting method is used to find appropriate values of  $a_2$  for which a phase-quantized, periodic solution exists. Once this is achieved, numerical simulations can easily be performed. Note that any integer value  $p$  is allowed as input for the phase quantization conditions, provided solutions exist for the parameter values. It turns out this imposes a lower bound on value of  $p$ . In the simulations, the actual value of  $p$  does not change whether the solution is stable or unstable. Increasing the phase-quantization integer  $p$  leads to a solution with a steeper phase profile, suggesting a more unstable situation. However, this phase effect is balanced by an increased offset  $a_2$  of the amplitude. Qualitatively, the dynamics are as depicted in Figs. 14–15. Thus the nontrivial phase solutions of Type B are stable for  $a_2 > 1/4$  and for  $0 < a_2 < \sqrt{1 - k^2}/4$ , whereas the nontrivial phase solution is unstable for  $a_2 < -1/4$ .

## IV. SUMMARY AND CONCLUSIONS

We considered the repulsive nonlinear Schrödinger equation with an elliptic function potential as a model for a trapped, quasi-one-dimensional Bose-Einstein condensate. Two new families of periodic solutions of this equation were found and their stability was investigated both analytically and numerically. Using analytical results for trivial phase solutions, we showed that solutions with sufficient offset are linearly stable. This is confirmed with extensive numerical simulations on the governing nonlinear equation. These conclusions also hold for solutions with nontrivial phase. Since we are modeling a Bose-Einstein condensate trapped in a standing light wave, our results imply that a sufficient number of condensed atoms (DC offset) is required to form a stable, periodic condensate.

To quantify this phenomena, we consider the  $k = 0$  limit and note that from Eqs. (1) and (13), the number of particles per well  $n$  is given by  $n = (\int_0^\pi |\psi(x, t)|^2 dx) / \pi = V_0/2 + B$ . In the context of the BEC, and for a fixed atomic coupling strength, this means a sufficient number

of condensed atoms per well  $n$  is required to provide an offset on the order of the potential strength. This ensures stabilization of the condensate. Alternatively, this solution can be interpreted as a sufficiently strong condensate for which the nonlinearity acts as a stabilizing mechanism.

**Acknowledgements:** We benefited greatly from discussions with William Reinhardt. The work of J. Bronski, L. D. Carr, B. Deconinck, and J. N. Kutz was supported by National Science Foundation Grants DMS-9972869, CHE97-32919, DMS-0071568, and DMS-9802920 respectively. K. Promislow acknowledges support from NSERC-611255

---

\* to whom correspondence should be addressed

- [1] G. Baym, *Lectures in Quantum Mechanics*, (Addison-Wesley, Redwood City, CA), Ch. 20.
- [2] J. C. Bronski, L. Carr, B. Deconinck, and J. N. Kutz, PRL
- [3] F. Dalfovo, S. Giorgini, L. P. Pitaevskii, and S. Stringari, Rev. Mod. Phys. **71**, 463 (1999).
- [4] L. D. Carr, M. A. Leung, and W. P. Reinhardt, J. Phys. B in press, e-print cond-mat/0004287 (2000).
- [5] M. Key *et al.*, Phys. Rev. Letts. **84**, 1371 (2000); N. H. Dekker *et al.*, Phys. Rev. Letts. **84**, 1124 (2000).
- [6] M. Kunze and *et. al*, Physica D **128**, 273 (1999); Y. S. Kivshar, T. J. Alexander, and S. K. Turitsyn, e-print cond-mat/9907475 (1999).
- [7] L. D. Carr, C. W. Clark, and W. P. Reinhardt, Phys. Rev. A in press, e-print cond-mat/9911177, cond-mat/9911178 (1999).
- [8] W. Ketterle, D. S. Sturfee, and D. M. Stamper-Kurn, in *Proceedings of the International School of Physics "Enrico Fermi"* (IOS Press, Amsterdam; Washington, D.C. 1999), pp. 67-176.
- [9] B. P. Anderson and M. A. Kasevich, Science **282**, 1686 (1998); E. W. Hagley *et al.*, Science **283**, 1706 (1999).
- [10] Y. B. Ovchinnikov *et al.*, Phys. Rev. Letts. **83**, 284 (1999).
- [11] D. Jaksch *et al.*, Phys. Rev. Letts. **81**, 3108 (1998); G. K. Brennen, C. M. Caves, P. S. Jessen, and I. H. Deutsch, Phys. Rev. Letts. **82**, 1060 (1999).
- [12] D.-I. Choi and Q. Niu, Phys. Rev. Letts. **82**, 2022 (1999).
- [13] S. Theodorakis and E. Leontidis, J. Phys. A **30**, 4835 (1997); F. Barra, P. Gaspard, and S. Rica, Phys. Rev. E **61**, 5852 (2000).
- [14] K. Berg-Sørensen and K. Mølmer, Phys. Rev. A **58**, 1480 (1998); M. J. Steel and W. Zhang, e-print cond-mat/9810284 (1998).
- [15] *Handbook of Mathematical Functions*, edited by M. Abramowitz and I. A. Stegun (National Bureau of Standards, Washington, D. C. 1964).
- [16] J. C. Bronski, L. D. Carr, R. Carretero-González, B. Deconinck, J. N. Kutz and K. Promislow, Phys. Rev. A, to be submitted (2000).
- [17] M. Weinstein, SIAM J. Math. Anal. **16**, 472 (1985).
- [18] *Algebro-geometric approach to nonlinear integrable equations*, E. D. Belokolos, A. I. Bobenko, V. Z. Enol'skii, A. R. Its and V. B. Matveev (Springer-Verlag, Berlin, 1994).
- [19] R. Courant and D. Hilbert, *Methods of Mathematical Physics*, (Wiley, New York, 1989).